The Astrophysical Journal, 875:75 (9pp), 2019 April 10 https://doi.org/10.3847/1538-4357/ab0e6a

The Population of Eccentric Binary Black Holes: Implications for mHz Gravitational-wave Experiments

Xiao Fang[1,2,3], Todd A. Thompson[3,4,5], and Christopher M. Hirata[2,3,4]

[1] Department of Astronomy and Steward Observatory, University of Arizona, Tucson, AZ 85719, USA; xfang@email.arizona.edu

[2] Department of Physics, The Ohio State University, Columbus, OH 43210, USA

[3] Center for Cosmology and AstroParticle Physics, Department of Physics, The Ohio State University, Columbus, OH 43210, USA

[4] Department of Astronomy, The Ohio State University, Columbus, OH 43210, USA

[5] Institute for Advanced Study, Princeton, NJ 08540, USA

Received 2019 January 30; revised 2019 March 6; accepted 2019 March 7; published 2019 April 17

Abstract

The observed binary black hole (BBH) mergers indicate a large Galactic progenitor population continuously evolving from large orbital separations and low gravitational-wave (GW) frequencies to the final merger phase. We investigate the equilibrium distribution of BBHs in the Galaxy. Given the observed BBH merger rate, we contrast the expected number of systems radiating in the low-frequency 0.1–10 mHz GW band under two assumptions: (1) that all merging systems originate from near-circular orbits, as may be indicative of isolated binary evolution, and (2) that all merging systems originate at very high eccentricity, as predicted by models of dynamically formed BBHs and triple and quadruple systems undergoing Lidov–Kozai eccentricity oscillations. We show that the equilibrium number of systems expected at every frequency is higher in the eccentric case (2) than in the circular case (1) by a factor of $\simeq$2–15. This follows from the fact that eccentric systems spend more time than circular systems radiating in the low-frequency GW bands. The GW emission comes in pulses at periastron separated by the orbital period, which may be days to years. For a LISA-like sensitivity curve, we show that if eccentric systems contribute significantly to the observed merger rate, then $\simeq$10 eccentric systems should be seen in the Galaxy.

Key words: globular clusters: general – gravitational waves – stars: black holes – stars: kinematics and dynamics

1. Introduction

The gravitational-wave (GW) experiments LIGO and VIRGO (Abbott et al. 2009; Accadia et al. 2012) recently made the first discoveries of binary black hole (BH) and neutron star (NS) mergers, and they are expected to detect many more such systems in future observing runs (Abbott et al. 2016a, 2016b, 2017a, 2017b, 2017c, 2017d; The LIGO Scientific Collaboration & the Virgo Collaboration 2018). Meanwhile, upcoming GW experiments, e.g., LISA (Amaro-Seoane et al. 2017), DECIGO (Kawamura et al. 2006), Taiji (Gong et al. 2015), and TianQin (Luo et al. 2016a) will focus on lower frequency ranges, and thus different types and evolutionary stages of compact object binaries.

Current high-frequency GW searches focus on binaries with circular orbits, which are expected both from isolated massive star binary evolution models and the circularization of the orbit during GW inspiral. Although the condition that the orbital eccentricity is small in the LIGO band may well be satisfied, it may not be true for systems at much lower frequency, where formation channels different from isolated binary evolution may imprint themselves (e.g., Sesana 2016; Chen & Amaro-Seoane 2017). In particular, two alternative channels for the production of merging compact object binaries have been suggested, and both predict large eccentricities ($e \gtrsim 0.9$) when the system is radiating GWs at low frequency ($\lesssim$1 mHz): (1) dynamically formed compact object binaries within and ejected from globular clusters (GCs) and other dense stellar systems (e.g., Rodriguez et al. 2016; Banerjee 2017, 2018a, 2018b; Chatterjee et al. 2017a, 2017b; Antonini et al. 2018; Arca-Sedda et al. 2018; D'Orazio & Samsing 2018; Fragione & Kocsis 2018; Gondán et al. 2018; Kremer et al. 2018, 2019; Rodriguez et al. 2018; Samsing & D'Orazio 2018) and (2) hierarchical triple and quadruple systems undergoing Lidov–Kozai (LK) eccentricity oscillations (e.g., Blaes et al. 2002; Miller & Hamilton 2002; Wen 2003; Thompson 2011; Antonini & Perets 2012; Naoz et al. 2013b; Antonini et al. 2016, 2017; VanLandingham et al. 2016; Petrovich & Antonini 2017; Silsbee & Tremaine 2017; Fang et al. 2018; Fragione et al. 2018; Hamers 2018; Hoang et al. 2018; Liu & Lai 2018; Randall & Xianyu 2018; Rodriguez & Antonini 2018). Note that the actual frequency range of the "highly eccentric" systems depends on the formation mechanism, and some mechanism can produce highly eccentric systems at even higher frequencies ($\gtrsim$10 mHz), e.g., the highly eccentric GW capture channel in clusters and the evection-induced migration in hierarchical systems.

Here, we argue that if the eccentric channels proposed account for the observed BBH merger rate, then there must be a large population of highly eccentric BBHs waiting to be discovered at low GW frequencies, in the 0.1–10 mHz band. In direct analogy with Socrates et al. (2012), who studied the population of tidally interacting high-eccentricity migrating hot Jupiters, in a steady state, the observed merger rate together with the continuity equation directly yields the number of eccentric BBH systems in the Galaxy. Since the periastron distance is directly related to the frequency of maximum GW power, these systems will appear as short pulses spaced in time by orbital period. Because the binary orbital angular momentum is approximately conserved at high eccentricity, the periastron distance and peak GW frequency are also nearly invariant during the high-eccentricity "migration" from large to small semimajor axes.

Here, we consider the possibility that a fraction of the observed LIGO events arise from a highly eccentric initial state. Assuming that the birth and death rates of BBHs are in equilibrium, the continuity equation yields the distributions of

orbital properties at every GW frequency, as BBHs evolve toward coalescence. We use the equilibrium assumption to derive the distributions of orbital elements for circular and highly eccentric systems. Because highly eccentric binaries spend more time radiating at a given GW frequency than a circular system with the same masses (Section 2), the equilibrium number of systems in the Galaxy is larger for eccentric systems than for circular systems if both channels contribute equally to the observed LIGO merger rate. Depending on the initial period (semimajor axis) distribution assumed for the eccentric channel, the equilibrium ratio of eccentric systems to circular systems in the ∼0.1–10 mHz band is ∼2–15. These eccentric systems have peak GW frequencies from 0.1 to 10 mHz, with orbital periods of the order of days or months, and Galactic systems can be detected by future GW interferometers.

In Section 2, we show analytically that the equilibrium number of eccentric systems should outnumber the equilibrium number of circular systems under generic assumptions. In Section 3, we calculate the distribution of BBHs as a function of GW frequency for several progenitor populations, including dynamically formed BBHs in dense stellar clusters, and triple systems undergoing LK oscillations. In all cases, we find an enhancement in the number of eccentric systems relative to circular systems in the 0.1–10 mHz band. In Section 4, we discuss the astrophysical implications of the possible existence of a large population of eccentric BBHs, and their detectability.

2. Circular versus Eccentric BBH Populations

Assuming that the birth and death rates of BBHs are in equilibrium, the continuity equation yields the distributions of orbital properties at every GW frequency, as BBHs evolve toward coalescence. Under this equilibrium assumption, the distribution of any quantity x is simply given by the chain rule

$$\frac{dN}{dx} = \frac{dN}{dt}\frac{dt}{dx} = \frac{\Gamma}{\dot{x}}, \tag{1}$$

where we have defined the steady "inflow" and "outflow" rate of systems as Γ.

For BBHs, the variations in the orbital parameters as the systems evolve depend sensitively on the eccentricity. The time-averaged evolution of the semimajor axis a and eccentricity e for a binary of masses m_1 and m_2 due to GW emission are (Peters 1964)

$$\langle \dot{a} \rangle = -\frac{64}{5}\frac{G^3 m_1 m_2 M}{c^5 a^3 (1-e^2)^{7/2}}\left(1 + \frac{73}{24}e^2 + \frac{37}{96}e^4\right), \tag{2}$$

$$\langle \dot{e} \rangle = -\frac{304}{15}e\frac{G^3 m_1 m_2 M}{c^5 a^4 (1-e^2)^{5/2}}\left(1 + \frac{121}{304}e^2\right), \tag{3}$$

where $M = m_1 + m_2$, G is the Newton's constant, and c is the speed of light.

For the circular binary case ($e = 0$), the frequency of the GWs, f, is set by the orbital period P, hence the semimajor axis a, i.e., $f = 2/P = 2\sqrt{GM/(4\pi^2 a^3)}$. Combining f with Equation (2), we obtain the time-averaged rate of increase in the GW frequency $\dot{f}/f = -3\dot{a}/(2a) = 96G^3 m_1 m_2 M/(5c^5 a^4)$. If the LIGO BH mergers are produced by initially circular binaries, there exists a distribution of circular BBHs at each a and f. If the distribution is in equilibrium, then the frequency distribution, dN/df, should be proportional to $dt/df = 1/\dot{f}$, and it is normalized by the merger rate Γ, i.e., (as in e.g., Farmer & Phinney 2003)

$$\left.\frac{dN}{df}\right|_{\rm circ} = \frac{\Gamma}{\dot{f}} = \frac{5\Gamma}{96}\frac{c^5}{G^3 m_1 m_2 M}\left(\frac{4GM}{4\pi^2}\right)^{4/3} f^{-11/3}. \tag{4}$$

For the eccentric binary case ($e > 0$), the GW frequency varies with period P, and the peak frequency f_p is set by the periastron distance $r_p = a(1-e)$, i.e., $f_p = 2\sqrt{GM/(4\pi^2 r_p^3)}$. The rate of increase in f_p is then $\dot{f}_p/f_p = -3\dot{r}_p/(2r_p)$. In the highly eccentric limit ($e \to 1$), we have

$$\dot{r}_p = -\frac{59}{3}\frac{1}{2^{7/2}}\frac{G^3 m_1 m_2 M}{c^5}\frac{1}{(a r_p)^{3/2}}, \tag{5}$$

$$\frac{\dot{f}_p}{f_p} = \frac{59}{2^{9/2}}\frac{G^3 m_1 m_2 M}{c^5}\frac{1}{(a r_p)^{3/2} r_p}. \tag{6}$$

The merger time for a highly eccentric BBH with initial periastron distance r_{p0} and semimajor axis a_0 can be estimated by

$$t_{\rm gw} \simeq \int_{r_{p0}}^{a_0}\frac{da}{|\dot{a}|_{e=1}} \simeq 1.20\times 10^7\ {\rm yr}\left(\frac{30^2\cdot 60\, M_\odot^3}{m_1 m_2 M}\right)\left(\frac{r_{p0}}{0.01\,{\rm au}}\right)^{7/2}\left(\frac{a_0}{\rm au}\right)^{1/2}. \tag{7}$$

Most of its time will be spent at its high initial eccentricity, when its periastron distance r_p and maximum GW frequency f_p are nearly invariant.

If the LIGO BH mergers arise from an initially highly eccentric BBH population, with a given a_0 and r_{p0}, assuming that the population is in equilibrium, then it will have a large peak in GW frequency near the initial $f_{p0} = 2\sqrt{GM/(4\pi^2 r_{p0}^3)}$. The indicated (density) distribution of systems near this frequency for the eccentric case should be much higher than that for the circular case:

$$\frac{(dN/d\log_{10} f)_{\rm ecce}}{(dN/d\log_{10} f)_{\rm circ}} = \frac{\dot{f}_{\rm circ}}{\dot{f}_{p,\rm ecce}} = \frac{96}{295}2^{9/2}\left(\frac{a_{0,\rm ecce}}{r_{p0}}\right)^{3/2} \simeq 7400\,\epsilon_{0,-2}^{-3/2}, \tag{8}$$

where $\epsilon_{0,-2} = (1-e_0)/10^{-2} = r_{p0}/a_{0,\rm ecce}/10^{-2}$, and where we have added the subscript "ecce" to denote the initial properties of the highly eccentric binary.

Note that the frequency distributions are different from the histograms of the number of systems binned in frequency. The ratio of the number of systems in the eccentric and circular cases near f_{p0} can be estimated by the ratio of merger times (since most of the merger time is spent near the initial orbital separation and frequency for both cases)

$$\left.\frac{N_{\rm ecce}}{N_{\rm circ}}\right|_{f_{p0}} \sim \left.\frac{t_{\rm gw,ecce}}{t_{\rm gw,circ}}\right|_{f_{p0}} \simeq \frac{\int_{r_{p0}}^{a_0} da/|\dot{a}|_{e=1}}{\int_0^{r_{p0}} da/|\dot{a}|_{e=0}} = \frac{3}{425}2^{23/2}\left(\frac{a_{0,\rm ecce}}{r_{p0}}\right)^{1/2} = 200\,\epsilon_{0,-2}^{-1/2}. \tag{9}$$

As an example, we take $m_1 = m_2 = 30\,M_\odot$, $a_0 = 1$ au, and $r_{p0} = 0.008, 0.015, 0.030, 0.068$ au, respectively, and calculate

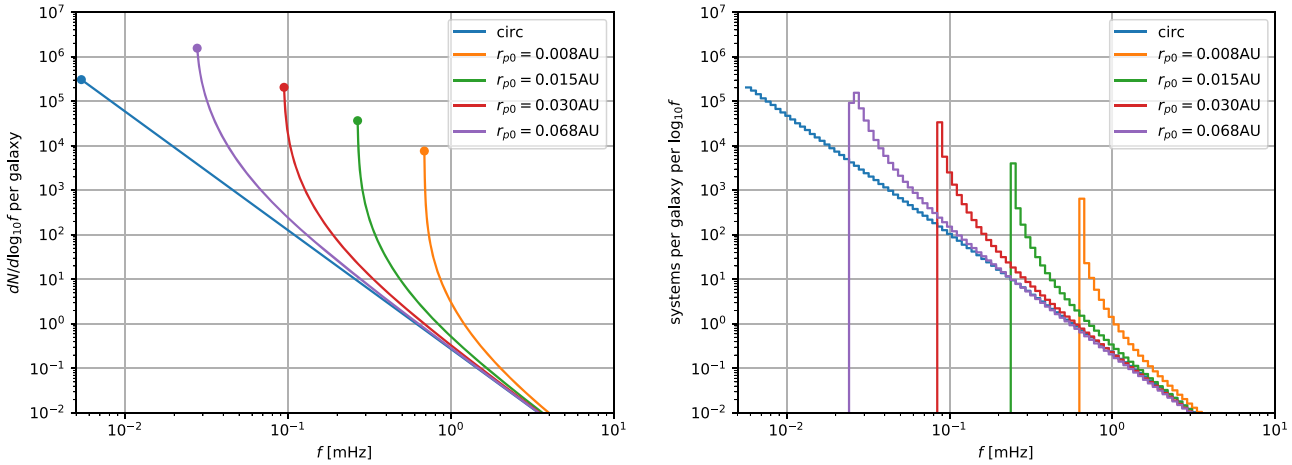

Figure 1. Left: frequency distributions ($dN/d\log_{10}f$) per Milky Way-sized galaxy, for cases where eccentric and circular merger rates are the same as the observed LIGO rate and the initial configurations for the eccentric populations are fixed at $a_0 = 1$ au, and $r_{p0} = 0.008, 0.015, 0.030, 0.068$ au, corresponding to merger times of $\simeq 6 \times 10^6$, 5×10^7, 6×10^8, and 10^{10} yr, respectively. The dots mark the initial values. For comparison, the circular case is shown with the blue line, which starts at $t_{\rm gw} = 10^{10}$ yr. Right: the corresponding peak frequency histograms normalized to per $\log_{10}f$ bin. The number of systems in each frequency bin is an integration of the distribution over that bin, which yields much smaller enhancement than the ratios of distributions as shown on the left, and strongly depends on the bin spacing. Also note that the huge enhancement ratios between eccentric and circular cases are highly peaked at initial frequencies and will be smeared out due to the broad distribution of realistic systems.

$\dot{f}_p$ as a function of f_p. Assuming each system represents a population of migrating binaries and that each population makes up the entire observed LIGO rate, we obtain the equilibrium distribution as $dN/d\log_{10}f = \Gamma \ln(10) f_p/\dot{f}_p$. This rate is normalized such that the total rate of mergers is equal to the observed LIGO BBH merger rate of $52.9^{+55.6}_{-27.0}\,{\rm Gpc^{-3}\,yr^{-1}}$ (Abbott et al. 2017a, 2017b, 2017c; The LIGO Scientific Collaboration & the Virgo Collaboration 2018). For illustration, we normalize to $50\,{\rm Gpc^{-3}\,yr^{-1}}$ throughout this paper. Since the Milky Way-size galaxy number density is roughly $0.01\,{\rm Mpc^{-3}}$, we have $\Gamma \sim 5 \times 10^{-6}\,{\rm yr^{-1}}$ per galaxy.

In Figure 1, we show the frequency distribution (left) and the number histogram (right) for the circular case (blue) compared to the eccentric sample populations (orange to purple, respectively). The dots in the left panel denote the starting position of each population. The implied enhancement in the equilibrium density of systems in the eccentric case relative to the circular case is very large, in accordance with Equation (8). Indeed, for $r_{p0} = 0.008$ au, the ratio of the eccentric population to the circular population is $>10^4$ at $\simeq 0.7$ mHz. However, the very highly peaked enhancement for individual system starting parameters shown in the left panel becomes more modest when we compute the number per frequency bin, as shown in the right panel, because eccentric systems spend most of their time radiating at a small range of GW frequency.[6] In addition, as we show below, a more realistic eccentric BBH population is more broadly distributed in frequency by the realistic joint distribution of (a_0, r_{p0}) provided by any given formation scenario. As we show below, these factors reduce the magnitude of the eccentric-to-circular enhancement, but Equations (8) and (9) show that it is generic for any secularly evolving eccentric merging BBH population that contributes at order unity to the observed LIGO rate.

[6] Note that the height of the histogram depends on the bin spacing and the enhancement ratio in each bin is higher than estimated by Equation (9), because Equation (9) assumes most of the systems are near f_{p0}, but the time a system (circular or eccentric) spent within one bin is much shorter than its merger time.

3. Results for Populations

In this section we give results for the equilibrium number of eccentric BBH systems in the Galaxy for several progenitor populations.

3.1. Simplest Population

To illustrate the scalings from Section 2 we assume a generic eccentric BBH population motivated by dynamically formed systems in dense stellar environments and few-body systems undergoing LK oscillations. We assume equal mass BBHs with $m_1 = m_2 = 30\,M_\odot$, an initial semimajor axis distribution that is log-uniform between 1 and 1000 au, and a thermal eccentricity distribution (Jeans 1919), i.e., e^2 is uniform in [0, 1]. Only systems with $t_{\rm gw}$ less than the Hubble time are included, since only these will contribute to the observed merger rate. The thermal eccentricity distribution is motivated by the properties of dynamically formed binaries produced in dense stellar systems (e.g., Samsing & D'Orazio 2018), and by the fact that it produces a uniform distribution of r_{p0} in the $e \to 1$ limit, equivalent to a uniform distribution of the angular momentum squared J^2, which is a natural consequence of non-secular stochastic angular momentum kicks due to the tertiary in hierarchical triple systems (e.g., Katz & Dong 2012).

We exclude systems from our sample with

$$r_p < 6.4 \times 10^{-5}\,{\rm au}\left(\frac{m_1 m_2 a}{30^2 M_\odot^2\,{\rm au}}\right)^{2/7}\left(\frac{M}{60M_\odot}\right)^{1/7}, \quad (10)$$

in the $e \to 1$ limit, because the fractional change in the orbital energy per orbit is of order unity and the secular equations break down (i.e., $t_{\rm gw} \leqslant P$). Such systems emit GWs at a peak frequency of

$$f_p > 0.95\,{\rm Hz}\left(\frac{30^2 M_\odot^2\,{\rm au}}{m_1 m_2 a}\right)^{3/7}\left(\frac{M}{60M_\odot}\right)^{2/7}. \quad (11)$$

These extreme systems are not of relevance for the main comparison in the LISA band from 0.1 to 10 mHz, but may

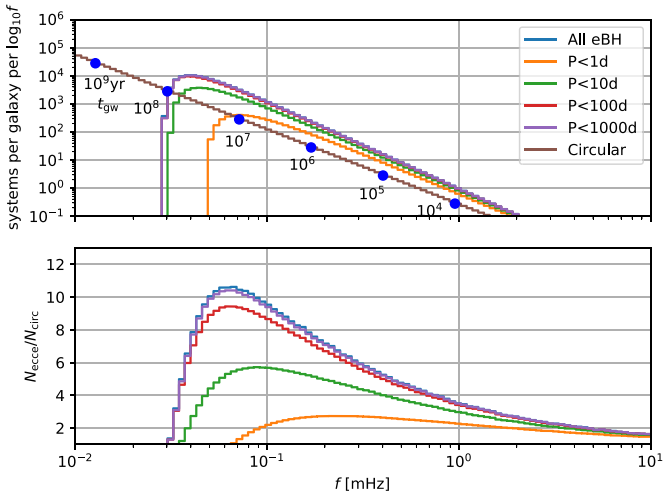

Figure 2. Upper: the peak frequency histograms of the simplest population of eccentric BBHs described in Section 3.1, normalized to per $\log_{10}f$ bin. The solid curves show the distributions of all the eccentric BBHs (labeled "All eBH") and those with orbital period $P < 1$, 10, 100, and 1000 days. The distribution for circular BBHs is also shown. Both the eccentric and circular channels are normalized to a merger rate of $\Gamma = 5 \times 10^{-6}\,\mathrm{yr}^{-1}$ per Milky Way-sized galaxy. The blue dots show the corresponding merger time $t_{\rm gw}$ of circular BBHs at each frequency. Lower: ratio of the number of eccentric systems to circular systems in each bin of frequency. An enhancement of 2–10 is seen in the frequency range $\simeq$0.04–3 mHz.

arise in nature (Silsbee & Tremaine 2017; Samsing & D'Orazio 2018; Kremer et al. 2019).

We evolve any given binary system "i" in the sample using the secular equations and calculate $\dot{f}_p^{(i)}$ as a function of f_p. We assume each system represents an equilibrium population with the same initial conditions undergoing migration toward coalescence. Thus, at any peak frequency, the population i has a distribution $dN^{(i)}/df_p \propto 1/\dot{f}_p^{(i)}$, and the total number of systems has a frequency distribution $dN/df = \sum_i dN^{(i)}/df_p = (\Gamma/N)\sum_i[1/\dot{f}_p^{(i)}]$, where N is the sample size, and the distribution is normalized to the LIGO rate of 50 $\mathrm{Gpc}^{-3}\,\mathrm{yr}^{-1}$. To obtain the number of systems N_{12} in frequency bin $[f_1, f_2]$, we integrate the frequency distribution over the bin, $N_{12} = (\Gamma/N)\sum_i t_{12}^{(i)}$, where $t_{12}^{(i)}$ is the time spent in the frequency bin for population i.

Figure 2 shows the histograms of systems in the frequency range [0.01, 10] mHz assuming that all the LIGO mergers come from either the eccentric channel or the circular channel. The upper panel shows the number of systems per logarithmic frequency bin, with the eccentric systems broken into subsamples by orbital period. For the BBH population we consider here, when $a > 11.5$ au, the orbital period exceeds 5 yr, which is roughly the operation timescale of LISA. Like single-transit planet detections in transit surveys (e.g., Villanueva et al. 2018), only a single pulse may be seen during the mission. However, systems with orbital periods of days or months will provide many repeated pulses during the entire mission (Section 4.1).

The bottom panel of Figure 2 shows the ratio of the number of eccentric systems to the number of circular systems in bins of frequency. Note that this ratio does not depend on the overall normalization of the LIGO rate. We find $\simeq$6–10 times more BBHs from the eccentric channel than that predicted by the circular channel at around 0.1 mHz, decreasing to $\simeq$2 times more at $\simeq$3 mHz. In absolute numbers, we find that $\simeq$45, 90, and 116 eccentric BBHs in our Galaxy are currently emitting in the 0.1–1 mHz range with orbital periods $P \leqslant 1$, 10, and 100 days, respectively. These numbers are $\simeq$2.5, 5, and 6.5 times more than that predicted from the circular case in the same frequency band.

The distribution of BBHs with frequency, and thus the enhancement with respect to the circular channel, depend on the initial distribution of (a_0, r_{p0}). For more realistic estimates, in Sections 3.2 and 3.2 we recompute the equilibrium distributions for eccentric BBHs arising from triple systems and dynamical interactions in GCs, respectively.

3.2. Distributions from Triple Systems

Binaries in hierarchical triple systems are subject to gravitational perturbations from their tertiaries, and can be driven to high eccentricities due to the LK mechanism (Kozai 1962; Lidov 1962). In secular calculations where both the inner and outer orbits are averaged, the time over which the angular momentum of the inner binary is changed by order unity by the tertiary (the instantaneous LK timescale), in the $m_2 \to 0$ limit, is given by (e.g., Bode & Wegg 2014; Antognini 2015)

$$t_{\rm LK}^{(\rm ins)} \sim \frac{8\sqrt{2}}{15\pi}\left(1+\frac{M}{m_3}\right)\frac{P_{\rm out}^2}{P}(1-e_{\rm out}^2)^{3/2}\sqrt{\frac{r_p}{a}}, \qquad (12)$$

where m_3 is the tertiary mass, and $e_{\rm out}$ and $P_{\rm out}$ are the eccentricity and the outer orbital period, respectively.

The equilibrium argument in Section 2 relies on the assumption of dynamically isolated binaries whose frequencies evolve monotonically as a result of GW emission. This is only true for triple systems whose inner binaries are dynamically decoupled from the outer tertiary. A criterion for decoupling is that the inner binary is driven to sufficiently high eccentricity that $t_{\rm LK}^{(\rm ins)}$ becomes longer than $t_{\rm gw}$ or the general relativistic (GR) precession timescale $t_{\rm prec} \sim 2c^2a^{3/2}r_p/[3(GM)^{3/2}]$.

In order to make a first estimate of the BBH population produced by triple systems, we run a secular calculation for triple systems with masses $m_1 = m_2 = m_3 = 30\,M_\odot$. The eccentricities of the inner and outer orbits, e and $e_{\rm out}$, are both sampled from a thermal distribution. The semimajor axis of the inner orbit a is sampled from a log-uniform distribution in [10,1000] au, and the semimajor axis ratio of outer to inner orbit, $a_{\rm out}/a$ is sampled from a log-uniform distribution in [10, 1000]. We discard systems with $a_{\rm out}(1-e_{\rm out}) < 10a$ to make sure the validity of the secular calculation, and discard systems with $a_{\rm out} > 10^5$ au because they are too wide to make up an important fraction of triple systems. The orientations of both the inner and outer orbits are sampled randomly. We turn on the quadrupole-order term in the Newtonian three-body perturbing Hamiltonian, which leads to the LK effect, the 1PN term (GR precession), and the 2.5PN GW dissipation terms for the inner orbit. We run 10^7 systems for 10 Gyrs, and find that $\sim$1.14% systems experience a decrease in their semimajor axis of order unity. These systems dynamically decouple from the tertiary and will merge within a relatively short time. We take the last eccentricity maximum of each such system and its semimajor axis a, and use them to set the initial conditions (a_0, r_{p0}) of "isolated binaries" in our calculation of the equilibrium distribution of the population.

Following the same procedure as in Section 3.1, we obtain the peak frequency histograms as shown in Figure 3. We again find a significant enhancement of the eccentric BBH population in

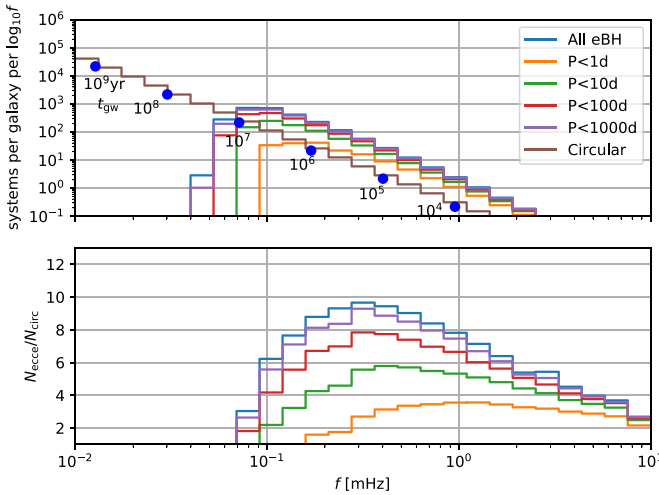

Figure 3. Same as Figure 2, but for the population of eccentric BBHs from secular dynamics of hierarchical triple systems described in Section 3.2. Upper: peak frequency histograms for eccentric and circular BBHs. Lower: ratio of eccentric to circular systems. A significant enhancement is seen in the frequency range 0.1–10 mHz. The total number of eccentric systems with orbital periods of days to months is expected to be of the order of 10–100.

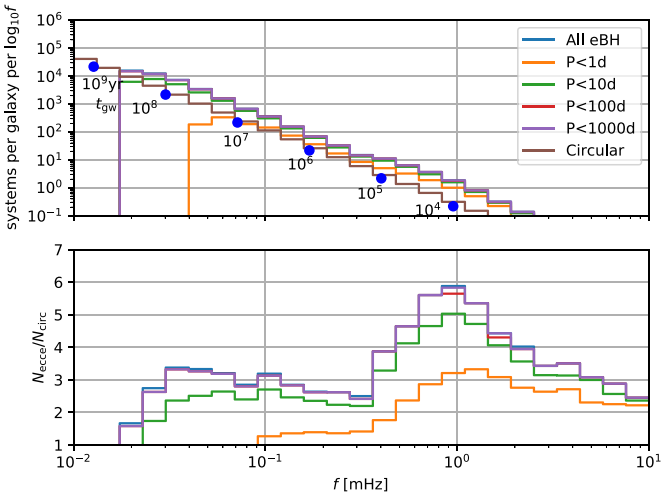

Figure 4. Same as Figures 2 and 3, but for the population of eccentric BBHs from GCs described in Section 3.2. Upper: peak frequency histograms for eccentric and circular BBHs. Lower: ratio of eccentric to circular systems. The "two-body" BBH mergers inside GCs dominate the peak in the distribution at $\simeq$0.4–10 mHz, while the "ejected" BBH mergers contribute over a broader frequency range (Kremer et al. 2019).

the frequency range 0.1–1 mHz, in which the absolute number of systems with orbital periods within $P \leqslant 1$, 10, and 100 days is $\simeq$20, 80, and 130. Compared to Figure 2, the systems at $f_p \lesssim 0.05$ mHz disappear. This comes from the fact that such systems still have perturbations from their tertiaries and are thus not dynamically isolated. However, the enhancement between 0.1 and 1 mHz persists, and is a factor of $\simeq$10 at $\sim$0.3 mHz.

Note that many triple systems undergoing LK oscillations may emit GWs in the $\simeq$0.1–10 mHz band, but may not be dynamically decoupled by our criterion. Such systems are not included here because they do not obey the equilibrium assumptions set out in Section 2. The total population of GW emitters in the 0.1–10 mHz band (whether dynamically decoupled or not) has yet to be computed for a realistic and evolving distribution of massive triple systems as the Galaxy forms over cosmic time.

Figure 3 gives just one minimal estimate for the distribution from triple systems. Different component binary masses, which lead to octupole-order terms in the three-body Hamiltonian, tertiary masses, initial orbital parameter distributions, and cuts on the resulting population can quantitatively affect the results. Several variations are presented in the Appendix, with maximum and minimum enhancements relative to the circular case of $\simeq$2–15.

3.3. Distributions from GCs

BBHs arising in GCs and other dense stellar environments provide another important channel for eccentric BH migration. Recent numerical studies show that three populations of BBHs are produced during few-body scattering in GCs. One is produced by chaotic three-body motion, leading to BBH mergers in the cluster at very high eccentricity such that $f_p \gtrsim 1$ Hz and $t_{\rm gw}$ becomes less than the orbital period P (as in Equation (10)). These systems evolve dynamically and never enter the 0.1–1 mHz band. A second physical class of mergers are those from BBHs excited to high enough eccentricity within the cluster that $t_{\rm gw}$ becomes shorter than the time between two interactions. The third class is those BBHs ejected from the cluster. Adopting the nomenclature of (Samsing & D'Orazio 2018) we refer to these three classes as "three-body mergers," "two-body mergers," and "ejected mergers," respectively. The latter two classes evolve secularly through the 0.1–1 mHz band and are dynamically isolated (Samsing & D'Orazio 2018; Kremer et al. 2019).

We set aside the dynamically merging three-body mergers and consider only two-body mergers and ejected mergers. As an illustration, for these two physical categories, we adopt the distribution of BBH parameters resulting from the semi-analytic model described in Samsing & D'Orazio (2018). The binary component masses are assumed equal, with $m = 30\,M_\odot$. The semimajor axis and eccentricity distributions for the BBHs when they are dynamically isolated are given by Samsing & D'Orazio (2018), and are used to set the initial conditions of "isolated binaries" in our calculation of the equilibrium BBH distribution, just as in Section 3.1.

Figure 4 shows the peak frequency histogram (top) and the ratio of eccentric to circular systems (bottom) for dynamically formed eccentric BBHs, normalized to the LIGO rate, as in previous figures. The shape of the number of systems per bin encodes the formation channel. As more clearly shown in the ratio plot (bottom), the two-body BBH mergers inside GCs dominate the distribution from 0.4–10 mHz, producing a peak relative to the circular case at $f_p \gtrsim 1$ mHz. The ejected BBH mergers resulting from binaries kicked out of GCs contribute to a much wider range of frequencies, with a low-frequency cutoff at $\simeq$0.02 mHz for the $P \gtrsim 10$ day binaries.

4. Discussion and Conclusion

Assuming the distribution of BBHs is in equilibrium, producing a steady merger rate as seen by LIGO, eccentric BBH formation channels predict a significantly different population distribution in GW frequency than for circular BBH formation channels. Because eccentric BBHs spend more time radiating in the 0.1–1 mHz GW band they should generically outnumber circular systems at the same frequency. We estimate that there are $\sim$10–100 systems with GW peak frequencies of 0.1–1 mHz in our Galaxy, which is $\simeq$2–10 times higher than that predicted for circular BBHs. Dozens of the

eccentric systems will have orbital periods of order days to months, implying they may be detectable.

4.1. Detectability

To estimate the two-detector sky-averaged signal-to-noise ratio (S/N) for eccentric BBHs, we start from Equation (45) in Barack & Cutler (2004), i.e., summing over contributions from all harmonics of the orbital frequency $f_{\rm orb}$,

$$\mathrm{S/N}^2 = 2\sum_{n=1}^{n_{\rm max}} \int \frac{h_{c,n}^2}{f_n S_h(f_n)} d\ln f_n , \quad (13)$$

where $n_{\rm max}$ is the maximum harmonic used in fitting, $f_n \equiv n f_{\rm orb}$, S_h is the full strain spectral sensitivity density including the LISA instrumental noise and the confusion noise from the unresolved galactic binaries (e.g., Robson et al. 2018).[7] The characteristic amplitude $h_{c,n}$ is given by $h_{c,n} = (\pi D)^{-1}\sqrt{2\dot{E}_n/\dot{f}_n}$, where the unit $G = c = 1$ has been applied. D is the distance of the source. $\dot{E}_n$ is the GW energy emission rate in the nth harmonic and is given by

$$\dot{E}_n = \frac{32}{5} M_c^{10/3} (2\pi f_{\rm orb})^{10/3} g_n(e), \quad (14)$$

where $M_c \equiv (m_1 m_2)^{3/5} M^{-1/5}$ is the chirp mass (for $m_1 = m_2 = 30\,M_\odot$, $M_c = 26\,M_\odot$), $g_n(e)$ is given by Equation (20) in Peters & Mathews (1963). Since the eccentric migration timescale ($\sim t_{\rm gw}$) is much longer than the mission lifetime τ, the orbital frequency does not change much during the mission, amd the integral in the S/N becomes

$$\int \frac{h_{c,n}^2}{f_n S_h(f_n)} d\ln f_n \simeq \frac{h_{c,n}^2}{f_n S_h(f_n)} \frac{\dot{f}_n \tau}{f_n} = \frac{2\dot{E}_n \tau}{\pi^2 D^2 f_n^2 S_h(f_n)}. \quad (15)$$

Combining it with Equation (14) we obtain

$$\mathrm{S/N}^2 = \frac{512\tau}{5D^2} \frac{(GM_c)^{10/3}}{c^8} (2\pi f_{\rm orb})^{4/3} \sum_{n=1}^{n_{\rm max}} \frac{g_n(e)}{n^2 S_h(f_n)} . \quad (16)$$

As discussed by Gould (2011) in the context of eccentric binary white dwarfs, the GW emission is dominated by pulses at periastron.

Taking $\tau = 4$ yr, $D = 10$ kpc, $n_{\rm max} = 10^5$, $f_p = 0.5$ mHz, $M_c = 26\,M_\odot$, for an eccentric BBH with $P = 1$, 10, and 100 days, we obtain S/N = 26, 8.5, and 2.7, respectively, implying that a number of eccentric BBHs will be detectable by LISA. In Figure 5, we show the S/Ns for systems at 10 kpc with different peak frequencies and $P = 1$, 10, and 100 days. Requiring S/N = 5(2) for detection and assuming a distance of 10 kpc (which gives a conservative estimate of the number of observable systems), we estimate that ~7, 7, and 8 (15, 17, and 17) eccentric BBHs with P less than 1, 10, and 100 days will be detected in our Galaxy in 0.1–1 mHz in the case of the simplest distribution, while ~5, 6, 7 (11, 14, 15) systems in the triple case, and ~4, 4, 5 (8, 9, 10) systems in the GC case. While the number of detectable eccentric systems is largely limited by the S/N at $f_p \lesssim 0.2$ mHz, where many more systems exist, the detection of the few systems at higher frequencies immediately implies the existence of the eccentric BBH population. Also note that although less systems are present at higher frequencies in our Galaxy, a larger volume is accessible due to the larger S/Ns, hence more extragalactic sources may be detectable (e.g., Rodriguez et al. 2018; Samsing & D'Orazio 2018; Kremer et al. 2019). These sources could also be interesting to experiments sensitive to slightly higher frequency bands, such as DECIGO, Taiji, and TianQin. The right axis of Figure 5 shows that eccentric systems with $P < 1$ day can be discovered by LISA out to ~8 Mpc distances.

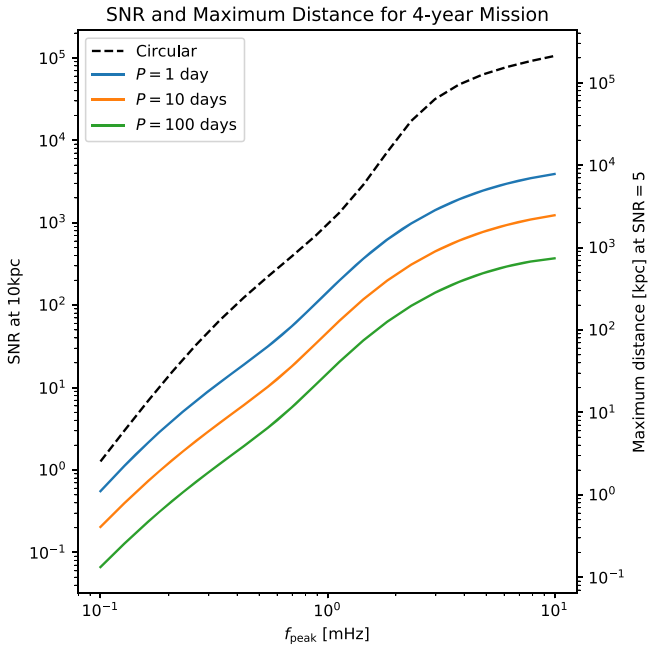

Figure 5. The left y-axis reads the estimated S/Ns for detecting eccentric BBH systems with $M_c = 26\,M_\odot$, $P = 1$, 10, 100 days, located at 10 kpc, in a 4 yr mission. The S/N scales proportionally with $\sqrt{\tau}/D$. The right y-axis reads the maximum distance for detecting these systems requiring S/N = 5. Note that the cosmological redshift is neglected, which only lowers the frequencies by 0.23% at 10 Mpc. For comparison, we also show the detectability of circular BBHs in the dashed line.

In Table 1, we show the estimated numbers of LISA-detectable galactic eccentric and circular BBHs, assuming different LIGO rates due to the uncertainty of the measured LIGO merger rate. Although the actual number of circular systems in each frequency bin is less than that of eccentric systems, the detectable numbers may be similar, due to the better S/Ns when detecting circular binaries. Note that the numbers are obtained by assuming all the systems are at distance 10 kpc, a typical value of their average distance. While closer systems have a higher S/N, much less systems exist at closer distances if a uniform spatial distribution of BBHs in the stellar halo is assumed, hence resulting in little changes in the estimated numbers of observable systems.

4.2. Complexities

A primary assumption in the results presented here is that the numbers of BBH systems are based on the equilibrium assumption, which will break down on 10 Gyr timescales. However, most of the eccentric migrating systems in triples and GCs with $f_p > 0.1$ mHz have merger times less than 1 Gyr, during which the variations expected as a result of the time history of star formation in the Galaxy may not be significant.

Additional uncertainties lie in the merger rate. There is a factor of a few uncertainty in the LIGO BBH merger rate, which is a function of BBH mass, and we have also assumed that the LIGO BBH merger rate applies to our Galaxy. While

[7] Note that the pre-factor "2," due to the fact that LISA has two channels, has been absorbed into S_h in Robson et al. (2018).

Table 1
The Estimated Numbers of LISA-detectable Galactic BBHs for a 4 yr Mission and for $S/N \geqslant 2$ and 5, Assuming All the LIGO BH Mergers Originate from the "Circular" Channel, the Simplest Eccentric BBH Population, the Triple Scenario, or the GCs

Γ (Gpc^{-3} yr^{-1})	25	50	100
		Circular	
$S/N \geqslant 2$	8	16	33
$S/N \geqslant 5$	6	11	23
		Simplest ($P < 1$, 10, 100 days)	
$S/N \geqslant 2$	8, 9, 9	15, 17, 17	30, 34, 35
$S/N \geqslant 5$	3, 4, 4	7, 7, 8	14, 15, 15
		Triple ($P < 1$, 10, 100 days)	
$S/N \geqslant 2$	5, 7, 7	11, 14, 15	22, 29, 30
$S/N \geqslant 5$	3, 3, 3	5, 6, 7	11, 13, 13
		GC ($P < 1$, 10, 100 days)	
$S/N \geqslant 2$	4, 5, 5	8, 9, 10	16, 19, 19
$S/N \geqslant 5$	2, 2, 2	4, 4, 5	8, 9, 9

Note. We scale the numbers for different LIGO BH merger rates Γ due to the uncertainties of the measured LIGO merger rate.

these uncertainties will affect the absolute numbers of systems expected, the ratios between the eccentric and circular cases presented are robust. In reality, the merger rate may be a mixture of all the possible channels. For the GC case, most of cluster simulations predict merger rates less than 50 Gpc^{-3} yr^{-1} (e.g., Rodriguez & Loeb 2018). Thus, the combined number of eccentric BBHs and their frequency distribution may depend on the fraction of each channel, which might in turn be used to probe the relative importance of various channels by LISA.

For the case of eccentric BBHs produced in triple systems, there are a number of uncertainties and complexities. These include (1) octupole-order perturbations for a realistic population, (2) evection, and (3) the astrophysics of realistic triple system masses and their evolution. The octupole-order perturbation (1) arises when the inner binary has unequal masses (e.g., Naoz et al. 2013a) and may change the frequency distributions as indicated in the tests in the Appendix. A more comprehensive analysis with a realistic BH mass distribution is needed to fully explore its effect. Evection (2) induces eccentricity oscillations of the inner orbit on timescale of $P_{\rm out}$, which may be important at high eccentricities where the inner orbit has small angular momentum, and is thus prone to torque from the tertiary (e.g., Ivanov et al. 2005; Katz & Dong 2012; Antognini et al. 2014; Fang et al. 2018). However, we neglect it here because evection may be considered as random kicks to the inner orbit and will produce a thermal distribution of e, which is already assumed in our initial distribution. Thus, while evection may change the absolute number of triple systems that produce merging and dynamically isolated BBHs, and while individual systems may experience non-secular changes of r_p, the overall distribution should not be modified by evection. The inclusion of evection may also introduce non-negligible secular effects when the triple systems are moderately hierarchical (e.g., Luo et al. 2016b; Grishin et al. 2018; Lei et al. 2018), which could suppress the octupole-order oscillations, and thereby affect the resulting distribution of systems as a function of GW frequency. Finally, (3) we neglect stellar evolution of the massive star progenitors, including possible mass transfer, adiabatic and dynamical mass-loss, and natal kicks due to the recoil during asymmetric supernova explosions. These effects may change the orbital parameter distributions or unbind the systems, which may suppress this formation channel (e.g., Silsbee & Tremaine 2017). Additionally, as the Appendix shows (see Run 3), a realistic distribution of tertiary masses can significantly change the relative enhancement of eccentric to circular systems.

4.3. Summary

Our major findings in this paper are as follows.

1. Assuming the distribution of BBHs is in equilibrium, producing a steady merger rate as seen by LIGO, we show that eccentric BBH formation channels predict a larger number of systems relative to circular BBH formation channels throughout the 0.1–1 mHz GW frequency band. Equations (8) and (9) and Figure 1 show that this predicted enhancement is generic, and follows from the fact that eccentric systems spend more time radiating in the low-frequency GW band than circular systems.
2. We estimate the absolute number of radiating systems in the circular and eccentric cases in the Galaxy. Figures 2–4 show the eccentric and circular cases for a generic eccentric population, for eccentric BBHs produced by triple systems undergoing Lidov–Kozai oscillations, and BBHs formed dynamically in GCs, respectively. Assuming that both eccentric and circular channels produce the observed LIGO rate, we find that eccentric systems outnumber circular systems by a factor of 2–10 throughout the 0.1−10 mHz GW band. Under these assumptions, there are ∼10–100 eccentric BBHs with GW peak frequencies of 0.1–1 mHz in the Galaxy. Dozens of these systems have orbital periods of the order of days to months.
3. Eccentric BBH systems emit GW pulses at periastron. We calculate the S/N for detecting eccentric binaries with a LISA-like sensitivity curve, and estimate that ≃7 (15) eccentric systems should be seen in the Galaxy with $S/N \geqslant 5(2)$, slightly less than the number of observable circular systems (11 and 16 for $S/N \geqslant 5$ and 2) in the range of 0.1–1 mHz. See Figure 5 and Table 1. For the rarer eccentric systems with higher peak GW frequency of 1–10 mHz, the detection volume increases to 0.8–8 Mpc for systems with orbital periods less than ≃1 day.

We thank Johan Samsing, Carl Rodriguez, Pierre Christian, and Paulo Montero for useful discussions, and Kyle Kremer for very detailed and helpful comments on the manuscript. We are also grateful for suggestions from an anonymous referee that improved the paper. X.F. is supported by the Simons Foundation and NSF 1313252. T.A.T. is supported in part by NSF 1313252, an IBM Einstein Fellowship from the Institute for Advanced Study, Princeton, and a Simons Foundation Fellowship. C.M.H. is supported by the Simons Foundation, the US Department of Energy, the Packard Foundation, NASA, and the NSF. Many computations in this paper were run on the CCAPP condo of the Ruby Cluster at the Ohio Supercomputer Center (Ohio Supercomputer Center 1987).

Appendix
Tests of Different System Configurations

In this appendix, we carry out tests for triple systems with different masses, initial orbital parameter distributions, and cuts. We summarize the runs (original and 5 tests) in Table 2.

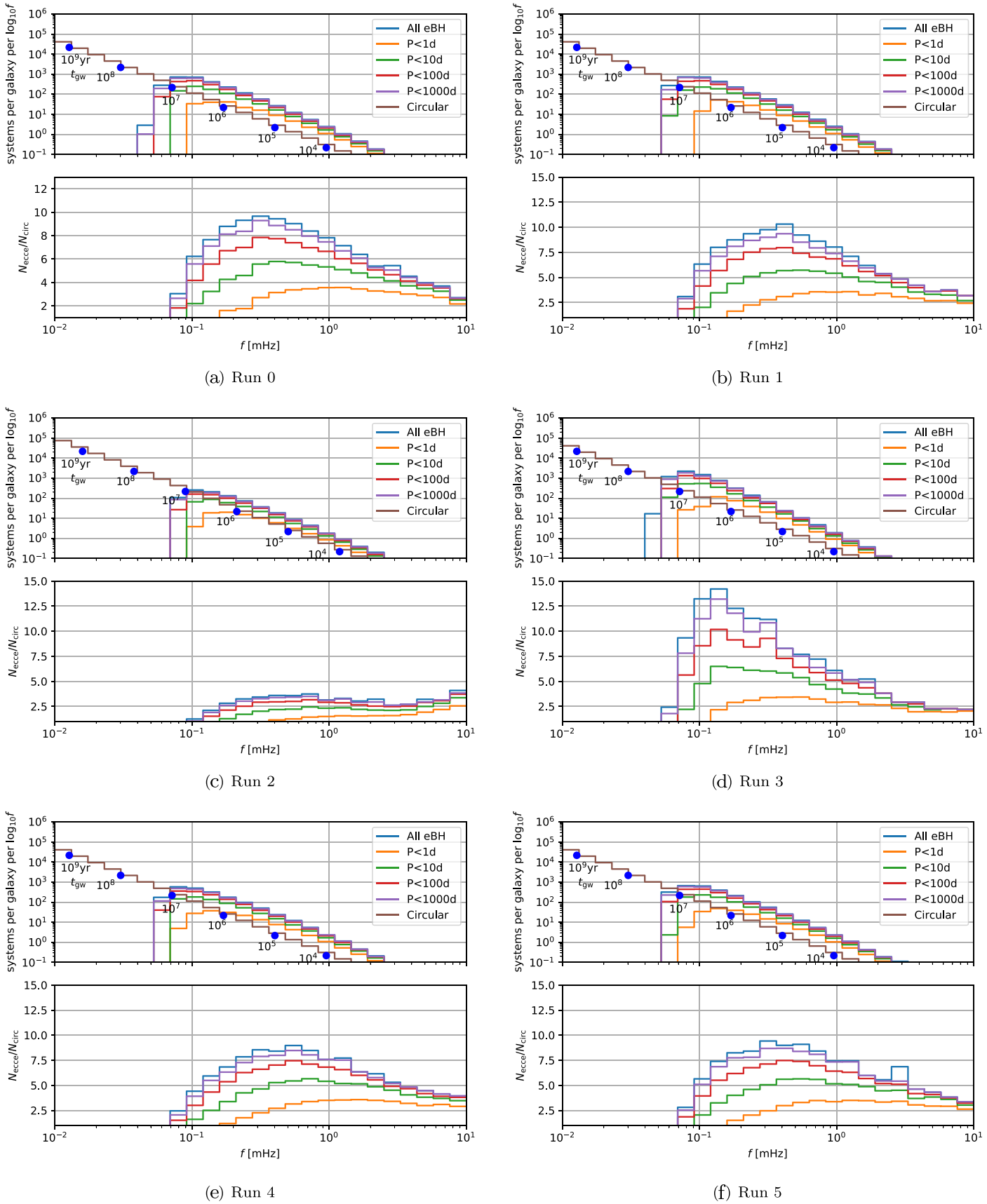

(a) Run 0 (b) Run 1

(c) Run 2 (d) Run 3

(e) Run 4 (f) Run 5

Figure 6. Peak frequency histograms from different runs listed in Table 2, normalized to per $\log_{10} f$ bin.

Table 2
The Settings of All the Triple System Runs

Runs	Masses ($M_\odot$)			a	Cuts	Merger Fractions in 10 Gyr
	m_1	m_2	m_3			
0	30	30	30	log-uniform	$a_{\rm out}(1-e_{\rm out})\geqslant 10a$	1.14%
1	30	30	30	log-normal	$a_{\rm out}(1-e_{\rm out})\geqslant 10a$	1.14%
2	30	15	30	log-uniform	$a_{\rm out}(1-e_{\rm out})\geqslant 10a$	2.73%
3	30	30	1	log-uniform	$a_{\rm out}(1-e_{\rm out})\geqslant 10a$	0.337%
4	30	30	30	log-uniform	$a_{\rm out}(1-e_{\rm out})\geqslant 5a$	1.40%
5	30	30	30	log-uniform	$a_{\rm out}(1-e_{\rm out})\geqslant 8a$	1.25%

Note. The inner semimajor axes a range from 10 to 1000 au. Note that run 0 is the original one in Section 3.2. Runs 1–5 are tests with 10^6 triple systems each. All the other settings not mentioned in the table are the same as run 0. Run 1 adopts a log-normal distribution for a, i.e., $\log_{10}(a)$ is assigned a mean of 1.7038 and a standard deviation of 1.52, inferred from Figure 13 in Raghavan et al. (2010). Run 2 has unequal binary masses, which turns on the octupole-order secular effect and enhances the merger fraction. Run 3 uses a small tertiary mass, which reduces the merger fraction due to weaker LK effect. Runs 4 and 5 adopt different cuts for the ratio between outer periastron and inner semimajor axis. Smaller ratio cuts (i.e., less hierarchical) lead to more systems with large tertiary perturbations, hence enhancing the merger fraction.

For each run, we use the orbital parameters of the mergers to produce the peak frequency histograms. The results are shown in Figure 6. All the runs except Run 2 have shown consistent enhancements in the 0.1–1 mHz frequency range. In Run 2, the curves move toward higher frequencies, because the inner binary mass is smaller (30+15 $M_\odot$), leading to a longer merger time, hence requiring a smaller initial periastron (larger initial peak frequency) to merge within 10 Gyr. Meanwhile, the octupole-order perturbation in the triples drives many systems to very high eccentricities (high f_p), as seen in Figure 6(c). In addition, the $\dot{f}$ for the corresponding circular case is smaller, resulting in a larger $dN/d\log_{10}f$ value. All the factors reduce the enhancement in the 0.1–1 mHz range.

ORCID iDs

Xiao Fang https://orcid.org/0000-0002-5054-9566

References

Abbott, B. P., Abbott, R., Abbott, T. D., et al. 2016a, PhRvL, 116, 061102
Abbott, B. P., Abbott, R., Abbott, T. D., et al. 2016b, PhRvL, 116, 241103
Abbott, B. P., Abbott, R., Abbott, T. D., et al. 2017a, PhRvL, 118, 221101
Abbott, B. P., Abbott, R., Abbott, T. D., et al. 2017b, ApJL, 851, L35
Abbott, B. P., Abbott, R., Abbott, T. D., et al. 2017c, PhRvL, 119, 141101
Abbott, B. P., Abbott, R., Abbott, T. D., et al. 2017d, PhRvL, 119, 161101
Abbott, B. P., Abbott, R., Adhikari, R., et al. 2009, RPPh, 72, 076901
Accadia, T., Acernese, F., Alshourbagy, M., et al. 2012, JInst, 7, 3012
Amaro-Seoane, P., Audley, H., Babak, S., et al. 2017, arXiv:1702.00786
Antognini, J. M., Shappee, B. J., Thompson, T. A., & Amaro-Seoane, P. 2014, MNRAS, 439, 1079
Antognini, J. M. O. 2015, MNRAS, 452, 3610
Antonini, F., Chatterjee, S., Rodriguez, C. L., et al. 2016, ApJ, 816, 65
Antonini, F., Gieles, M., & Gualandris, A. 2018, arXiv:1811.03640
Antonini, F., & Perets, H. B. 2012, ApJ, 757, 27
Antonini, F., Toonen, S., & Hamers, A. S. 2017, ApJ, 841, 77
Arca-Sedda, M., Li, G., & Kocsis, B. 2018, arXiv:1805.06458
Banerjee, S. 2017, MNRAS, 467, 524
Banerjee, S. 2018a, MNRAS, 481, 5123
Banerjee, S. 2018b, MNRAS, 473, 909
Barack, L., & Cutler, C. 2004, PhRvD, 70, 122002
Blaes, O., Lee, M. H., & Socrates, A. 2002, ApJ, 578, 775
Bode, J. N., & Wegg, C. 2014, MNRAS, 438, 573
Chatterjee, S., Rodriguez, C. L., Kalogera, V., & Rasio, F. A. 2017a, ApJL, 836, L26
Chatterjee, S., Rodriguez, C. L., & Rasio, F. A. 2017b, ApJ, 834, 68
Chen, X., & Amaro-Seoane, P. 2017, ApJL, 842, L2
D'Orazio, D. J., & Samsing, J. 2018, MNRAS, 481, 4775
Fang, X., Thompson, T. A., & Hirata, C. M. 2018, MNRAS, 476, 4234
Farmer, A. J., & Phinney, E. S. 2003, MNRAS, 346, 1197
Fragione, G., Grishin, E., Leigh, N. W. C., Perets, H. B., & Perna, R. 2018, arXiv:1811.10627
Fragione, G., & Kocsis, B. 2018, PhRvL, 121, 161103
Gondán, L., Kocsis, B., Raffai, P., & Frei, Z. 2018, ApJ, 860, 5
Gong, X., Lau, Y.-K., Xu, S., et al. 2015, JPhCS, 610, 012011
Gould, A. 2011, ApJL, 729, L23
Grishin, E., Perets, H. B., & Fragione, G. 2018, MNRAS, 481, 4907
Hamers, A. S. 2018, MNRAS, 478, 620
Hoang, B.-M., Naoz, S., Kocsis, B., Rasio, F. A., & Dosopoulou, F. 2018, ApJ, 856, 140
Ivanov, P. B., Polnarev, A. G., & Saha, P. 2005, MNRAS, 358, 1361
Jeans, J. H. 1919, MNRAS, 79, 408
Katz, B., & Dong, S. 2012, arXiv:1211.4584
Kawamura, S., Nakamura, T., Ando, M., et al. 2006, CQGra, 23, S125
Kozai, Y. 1962, AJ, 67, 591
Kremer, K., Chatterjee, S., Breivik, K., et al. 2018, PhRvL, 120, 191103
Kremer, K., Rodriguez, C. L., Amaro-Seoane, P., et al. 2019, PhRvD, 99, 063003
Lei, H., Circi, C., & Ortore, E. 2018, MNRAS, 481, 4602
Lidov, M. L. 1962, P&SS, 9, 719
Liu, B., & Lai, D. 2018, ApJ, 863, 68
Luo, J., Chen, L.-S., Duan, H.-Z., et al. 2016a, CQGra, 33, 035010
Luo, L., Katz, B., & Dong, S. 2016b, MNRAS, 458, 3060
Miller, M. C., & Hamilton, D. P. 2002, MNRAS, 330, 232
Naoz, S., Farr, W. M., Lithwick, Y., Rasio, F. A., & Teyssandier, J. 2013a, MNRAS, 431, 2155
Naoz, S., Kocsis, B., Loeb, A., & Yunes, N. 2013b, ApJ, 773, 187
Ohio Supercomputer Center 1987, Ohio Supercomputer Center (Columbus, OH: Ohio Supercomputer Center), http://osc.edu/ark:/19495/f5s1ph73
Peters, P. C. 1964, PhRv, 136, 1224
Peters, P. C., & Mathews, J. 1963, PhRv, 131, 435
Petrovich, C., & Antonini, F. 2017, ApJ, 846, 146
Raghavan, D., McAlister, H. A., Henry, T. J., et al. 2010, ApJS, 190, 1
Randall, L., & Xianyu, Z.-Z. 2018, ApJ, 864, 134
Robson, T., Cornish, N., & Liu, C. 2018, arXiv:1803.01944
Rodriguez, C. L., Amaro-Seoane, P., Chatterjee, S., et al. 2018, PhRvD, 98, 123005
Rodriguez, C. L., & Antonini, F. 2018, ApJ, 863, 7
Rodriguez, C. L., Chatterjee, S., & Rasio, F. A. 2016, PhRvD, 93, 084029
Rodriguez, C. L., & Loeb, A. 2018, ApJL, 866, L5
Samsing, J., & D'Orazio, D. J. 2018, MNRAS, 481, 5445
Sesana, A. 2016, PhRvL, 116, 231102
Silsbee, K., & Tremaine, S. 2017, ApJ, 836, 39
Socrates, A., Katz, B., Dong, S., & Tremaine, S. 2012, ApJ, 750, 106
The LIGO Scientific Collaboration, & the Virgo Collaboration 2018, arXiv:1811.12907
Thompson, T. A. 2011, ApJ, 741, 82
VanLandingham, J. H., Miller, M. C., Hamilton, D. P., & Richardson, D. C. 2016, ApJ, 828, 77
Villanueva, S., Jr., Dragomir, D., & Gaudi, B. S. 2018, arXiv:1805.00956
Wen, L. 2003, ApJ, 598, 419